Quantum wells in tilted fields: Semiclassical analysis and experimental evidence for effects ''beyond'' periodic orbits

D. S. Saraga and T. S. Monteiro
Department of Physics and Astronomy, University College, University of London, Gower Street, London WC1E 6BT, United Kingdom
(Received 28 May 1997; revised manuscript received 10 October 1997)

Quantum wells in tilted fields are of great current interest as experimental probes of the transition to chaos in a mesoscopic system. Here we carry out an analysis of quantal and experimental periodic orbit (PO) amplitudes for tilt angles $\theta = 11°$ and 27°. We calculate stability parameters and test the quantal and experimental results against a recently proposed theoretical periodic orbit formula. We find that many experimental features are understood in terms of torus states, ghosts, and bifurcations rather than isolated periodic orbits. We analyze previously unexplained jumps in period-one current at low fields and show these to be due to the changes in the quantum number of the most accessible torus state. We estimate that about one-quarter of the I-V oscillations in these experiments are dominated by ghost contributions (complex periodic orbits). We find that only a small fraction of bifurcations of accessible periodic orbits are visible experimentally. Agreement with the simplified PO formula is only qualitative and the limitations of the theory are discussed. [S1063-651X(98)12804-0]

PACS number(s): 05.45.+b, 03.65.Sq, 73.20.Dx

I. INTRODUCTION

The magnetotunneling spectrum of the resonant tunneling diode (RTD) is a new experimental probe of quantum chaos. Oscillations in the current-voltage (I-V) traces have been associated with the effects of unstable periodic orbits [1]. This system has been the subject of several recent theoretical and experimental studies, e.g., [2–7]. For example, experiments reported in [2] investigated the transition between regularity and chaos. They measured a large number of I-V traces for many values of the magnetic field and of the tilt angle θ between the applied voltage and the magnetic field, enabling one to exploit the scaling properties of the classical dynamics.

Quantum calculations of the tunneling current have been performed, e.g., [5,6] where fully quantal I-V traces were calculated and compared with experiment. In [4,6] *scaled* quantum solutions of the problem were developed for fixed classical dynamics. A model for the tunneling probability was developed that showed that, for weak tunneling, the relative amplitudes of the periodic orbit oscillations are insensitive to the barrier shapes. In [6] it was shown that the scaled quantum spectra can be used to obtain characteristic line profiles corresponding to specific classical dynamical regimes in the experiment.

Although such studies have already exposed a number of interesting dynamical regimes including bifurcation effects, e.g., [2–7], many experimental features remain poorly understood. Some of the interpretation of data is still controversial [8–10].

The major gap in understanding is the absence of a widely accepted quantitative theory for the semiclassical current. In the case of the archetypical example of quantum chaos, the atom in a magnetic field, a semiclassical theory for the photoabsorption — closed orbit theory (distinct from the Gutzwiller trace formula) — has been developed and shown to give excellent results for hydrogen and other atoms [11–15].

For the case of the RTD it is clear from past work that the contribution from a periodic orbit (PO) p to the current is determined mainly by two factors: (1) a tunneling propensity W_p encompassing information about the accessibility of the PO to electrons tunneling from the 2DEG (the electronic state prior to tunneling) and (2) classical properties of the PO such as the elements of its two-dimensional stability matrix M_p.

Recently a semiclassical theory was proposed in [16]. In this theory the current is weighted by $\sqrt{1/m_{21}}$ where m_{21} is an off-diagonal element of M_p. In contrast, we note that the weighting for the atomic theory of photoabsorption [12] is $\sqrt{1/m_{12}}$ so is related to the *other* off-diagonal element of the monodromy matrix.

An aim of this work is to place constraints on semiclassical theories by carrying out a careful quantitative analysis of experimental and quantal PO amplitudes. We also carry out a stability analysis of the accessible POs. We use these to test the validity of the periodic orbit theory proposed in [16].

Our main finding here is that most of the experimental data cannot be understood in terms of contributions from the close vicinity of isolated POs (the regime of the Gutzwiller trace formula). In the regime dominated by a large stable island, the experiments show a sequence of ''jumps'' in the period-one current. We attribute these to the effects of torus quantization; the accessibility of outer torus states of a large stable island can differ greatly from the accessibility of states localized on the central PO. The jumps occur as the quantum number of the most accessible states steps up through a series of $K = 0,1,2,\ldots$ tori. We propose a simple model based on Miller quantization that gives excellent agreement with quantal calculations.

In addition we find two wide ranges covering over one-quarter of the I-V traces where there are substantial quantal and experimental current oscillations but there is no real or accessible periodic orbit that could account for the results. We attribute these oscillations mainly to ''ghost'' contribu-

tion since they lie below tangent bifurcations. However, ghost contributions should decay exponentially below a bifurcation and the reason why these contributions persist so far below the bifurcation remains poorly understood.

We find many bifurcations, only a few of which are significant in the experiment. The reasons that some bifurcations are visible experimentally and others are not (even when the PO is accessible to the tunneling electrons) are analyzed.

We find agreement with the semiclassical theory of [16] is at best qualitative. The reasons for the discrepancies are discussed.

In Sec. II we discuss the device and the quantal calculations, including the inverse $\hbar$ spectroscopy, which we use to calculate ''periodic orbit'' amplitudes from quantal calculations. In Sec. III we discuss the experimental data reduction, which we use to obtain and normalize experimental amplitudes. In Sec. IV we describe the semiclassical theory and the calculation of semiclassical amplitudes. In Sec. V we analyze the classical stability and the important bifurcations. We show surfaces of section and give a qualitative discussion of the relative importance of accessibility versus stability for the main POs. In Sec. VI we present an analysis of the experimental oscillations. In Sec. VII the results of the comparison between quantal, semiclassical, and experimental amplitudes are presented. In Sec. VIII we present a model and calculations for the stable torus-quantization regime. Finally, we present our conclusions and summarize our findings.

II. THE RTD PROBLEM: QUANTUM SPECTRUM

The resonant tunneling diode [1] problem consists of a single quantum well with barriers at $x=0$ and $x=L$, acted on by an electric field $\mathbf{F}$ along the x axis (directed towards negative x) due to an applied voltage V and a magnetic field of strength B, tilted at an angle θ to $-\mathbf{F}$ in the x-z plane. Electrons tunnel in through the emitter barrier $x=0$ from an outer two-dimensional electron gas (2DEG) accumulation layer and out through the collector barrier at $x=L$, resulting in a current $I(V)$. The dynamics within the well can be reduced to a 2D motion in the x-z plane, which is described by the Hamiltonian

$$H=E=\frac{1}{2m}(p_x^2+p_z^2)+\frac{B^2e^2}{2m}(x\sin\theta-z\cos\theta)^2-eFx$$

with specular bounces at the barriers. In atomic units $\hbar=1$ and the electrons have a charge $e=+1$ and a mass $m\simeq 0.067$.

The major reason the analogous atom in a field system has proved to be such a powerful probe of quantum chaos is that it has a classical scaling property that enabled detailed quantitative comparisons with semiclassical periodic orbit type theories. The RTD also has such a property and its effectiveness in the calculation of quantum currents has been demonstrated [6].

Classical scaling in the low E limit has been found in [3]. For arbitrary E, by rescaling momenta and position through $\tilde{p}=p/B$ and $\tilde{q}=q$, one can show [6] that, for fixed θ, the classical dynamics depends only on $\mathcal{R}=E/FL$, $\rho=B^2L/mF=L/m\epsilon$ where $\epsilon=F/B^2$. The dimensionless parameters $\mathcal{R}$ and ρ represent the ratio of, respectively, the injection energy and the diamagnetic energy inside the well to the potential energy due to the bias voltage. The voltage drop across the well FL is approximately equal to the applied voltage V across the whole device (well plus barriers): $FL\simeq V$. In the experiments $L=120$ nm and $\mathcal{R}\simeq 0.15$ are constant. Hence we investigate simply the dynamical behavior as a function of $\epsilon=F/B^2$ for each θ.

In our previous work we demonstrated that the quantum spectrum and the experiments can exploit this scaling property. For example, the classical action along a trajectory becomes

$$S(E,F,B)=\int p\,dq=B\int \tilde{p}\,d\tilde{q}=B\tilde{S}(\mathcal{R},\epsilon), \qquad (1)$$

which implies that B^{-1} plays the role of an effective Planck constant. Below we use the notation $p\rightarrow p/B$.

We solve the scaled and ''rearranged'' Schrödinger's equation at fixed $\mathcal{R}$ and fixed ϵ [6]:

$$\{(\tilde{x}\sin\theta-\tilde{z}\cos\theta)^2-2m\epsilon(\tilde{x}+\mathcal{R}L)\}\psi_i=\frac{1}{B_i^2}\nabla^2\psi_i\,.$$

In this case, the (generalized) eigenvalues B_i are the magnetic field values. Because of the classical scaling, all states correspond to the same classical dynamics. As the action scales with B, as seen in Eq. (1), the effect of classical orbits appears in the semiclassical spectrum of B_i as modulations of constant frequencies, given by their scaled action $\tilde{S}(\epsilon)$. We can use Fourier transforms (FT) of $I(B)$ to ''invert'' a quantum spectrum and obtain the frequencies, as well as the amplitudes A_p^{QM}, for the pth PO contribution to the current. This technique is sometimes termed inverse $\hbar$ spectroscopy, since a FT is carried out with respect to $\hbar^{-1}$. The frequencies, which can be obtained to within 1% accuracy, allow us in many cases to distinguish different PO contributions to the current.

Our Fourier transforms of the spectra were actually carried out with respect to a rescaled magnetic field N defined by $N=BL\sqrt{2mL\epsilon(\mathcal{R}+1/2)}/\pi\hbar$. This rescaled field provides a more convenient unit for the action since then a period-one current corresponds to an orbit of action close to unity.

Calculation of the current requires weighting the density of states by the tunneling probabilities:

$$I(N)=\sum_i |\mathbf{W}_i|^2\delta(N-N_i).$$

For weak tunneling the $\mathbf{W}_i$ may be obtained from the Bardeen Hamiltonian transfer matrix [17], which gives the coupling between an initial state ϕ_0, i.e., the solution on the left of the emitter wall for the separable limit, with the ψ_i. The ϕ_0 are generally in the lowest in-plane Landau state $l=0$. With that assumption, our $\mathbf{W}_i$ depend only on the $l=0$ component of the eigenstates in the well. In [6] we proposed a simplified tunneling model, which was shown to yield results proportional to the Bardeen values — to within a smooth global envelope — in the case of weak tunneling. Here we have extended those calculations considerably.

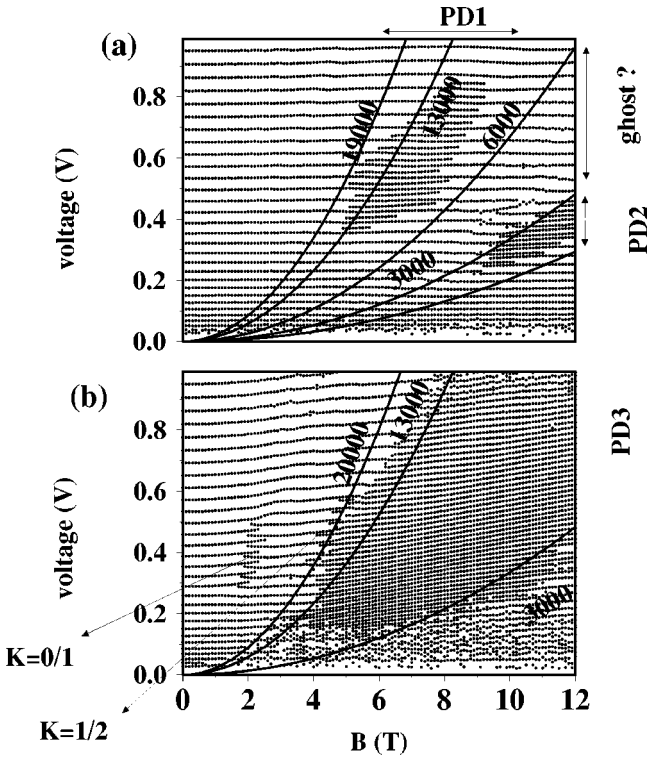

FIG. 1. Experimental data plotting the positions of maxima in the $I(V)$ traces as a function of magnetic field B. The curves are parabolas of constant V/B^2, which correspond approximately to constant classical dynamics. They are labeled with the value of $\epsilon = F/B^2$. PD1, PD2, and PD3 denote period-doubling regions. The features associated with the changeover of the quantum number of the torus series with the strongest current amplitude are indicated by the torus K quantum numbers. (a) $\theta = 11°$. (b) $\theta = 27°$.

About 100 000 eigenstates were calculated at different ϵ for $\theta = 11°$ and 27°. All quantum states corresponding to an applied voltage $V \simeq FL$ in the range 0.1–1.1 V were obtained. This voltage range corresponds also to N in the range $N \sim 12-42$. Hence the average effective $\hbar = 1/N \sim 1/27$ for all our quantum amplitudes. The precise number of states in this range varied with ϵ but ranged from 500 to 2000 states for different ϵ. We then used inverse-$\hbar$ spectroscopy to obtain the period-one and period-two current amplitudes A^{QM}, from the quantum spectra, as a function of ϵ.

III. EXPERIMENTAL DATA REDUCTION

Because of the classical scaling, the curves of constant classical dynamics should lie along parabolas of constant V/B^2. Some of these parabolas are shown in the experimental ''fan'' diagrams of [2] reproduced in Fig. 1. Here the maxima in the current oscillations are plotted as a function of magnetic field for $\theta = 11°$ and 27°. Two period-doubling regions (PD1 and PD2) stand out clearly at 11°. A single large region (PD3) dominates most of the 27° experiment. We indicate also two smaller regions, which we denote $K = 0 -1,1-2$ where the period-one current jumps abruptly. These are shown below (see Sec. VIII) to be due to the effect of changes in quantum number K of the torus state, which dominates the current. Similar features were seen in experiments at other tilt angles.

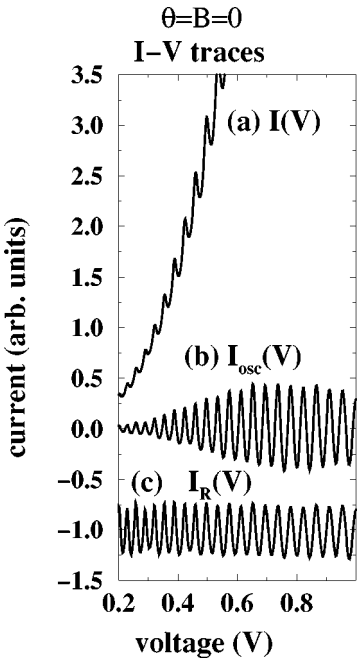

FIG. 2. Normalization of experimental data: Current-voltage plots for $\theta = B = 0$. (a) Raw trace $I(V)$. (b) Oscillating current $I_{\mathrm{osc}} = I - I_{\mathrm{sm}}$ where the smooth term I_{sm} has been subtracted. (c) Reduced current $I_R = I_{\mathrm{osc}}/G(E)$ where the global tunneling envelope $G(E)$ has been eliminated.

In previous work e.g., [2,6,7] the analysis concentrated on explaining the position, i.e., the V-B range occupied by these features, mainly in terms of bifurcations. The amplitudes of the experimental oscillations were not considered. In other work, the experimental d^2I/dV^2 was plotted [5] since differentiating $I(V)$ enhances its oscillatory character.

Here we suggest a procedure for extracting the experimental amplitudes from the data in order to compare directly with semiclassical and quantal PO amplitudes.

There are of course many uncertainties in the experimental parameters. However, because the classical dynamics depend only on two dimensionless scaled parameters these will only smoothly distort or displace the parabolas. Such effects appear as a displacement between our quantum results and the corresponding experimental feature. For instance, the applied voltage is proportional but not equal to FL. There may also be variations in the effective mass, which is voltage dependent: $m = 0.067 f(V)$. In this case, since m appears only as the product mV a change in m appears as a displacement in the value of the voltage corresponding to a certain behavior. We circumvented this problem in part by considering theoretical data for most possible values of the parameters spanned by the experiment, and hence identifying the slightly displaced features.

The experimental resolution is limited by inelastic processes and also, at high V, by coupling to the continuum due to the finite height of the barriers: there is a voltage dependence to the linewidth even for $B = 0$. This effect was investigated in [6] where the width of the $B = 0$ trace was used to estimate a voltage-dependent broadening.

In Fig. 2 we demonstrate how we analyze the data in terms of a reduced spectrum. In (a) a raw $I(V)$ trace is shown for the $\theta = B = 0$ case. In (b) we show $I_{\mathrm{osc}} = I - I_{sm}$

where the smooth term I_{sm} has been subtracted. This leaves only the oscillating (PO) contributions, convolved with a smooth, global energy-dependent envelope $G(E)$ with $E \simeq \mathcal{R}V$. At $B=0$ one would expect only a single period-one contribution due to straight-line motion bouncing back and forth between the walls. $G(E)$ is due simply to the details of the tunneling and the initial state on the left of the emitter barrier. For higher voltage there is substantial coupling to the continuum due mainly to escape over the second barrier. Our theoretical calculations also yield a smooth envelope, which is dynamically uninteresting. For the theory it is simply proportional to B^2 [6] so it is easily eliminated.

In the experiment we estimate this from the $\theta=0°$ traces. For $B=0-5$ T, $G(E)$ is insensitive to B. For higher fields the position and height of the maximum of $G(E)$ as seen in Fig. 2(b) depends on B for voltages $V>0.6$ V. We have estimated the experimental envelope $G(E)$ to be one of the traces at $\theta=0°$, and have normalized the experiments using the $\theta=0°$, $B=4.9$ T envelope.

This procedure allows us to compare experimental results with our calculated quantal periodic orbit amplitudes, which we also normalize to the corresponding theoretical period-one oscillations at $\theta=0°$. Figure 2(c) shows the resultant reduced spectrum $I_R=I_{\rm osc}/G(E)$, which for $\theta=0$ gives period-one oscillations of equal height. Hence, for other regimes we can attribute changes in the theoretical or experimental *reduced* spectra I_R as being due to, essentially, changes in either the accessibility W_p or the stability M_p. We estimate that uncertainties in $G(E)$ introduce an uncertainty of order $10-20\%$ for $V<0.6$ V and to less than a factor of 2 for $V>0.6$ V.

IV. SEMICLASSICAL THEORY

The derivation of the semiclassical theory is described in [16] for both a general current operator as well as the simple Bardeen matrix element. Here we review its application to the Bardeen matrix element only briefly and explain the minor modifications required by our scaling.

The current takes the form

$$I(E)\propto\sum_i \left| \int dz \left\{ \varphi^*(x,z)\frac{\partial\psi_i}{\partial x}(x,z) - \psi_i(x,z)\frac{\partial\varphi^*}{\partial x}(x,z)\right\}\right|^2_{x=\bar{x}} \delta(E-E_i),$$

where the initial state has the separable form [6] $\varphi(x,z)=\chi(x)\phi_0(z)$ and $\bar{x}$ is a fixed point in the first barrier used for the Bardeen matrix element. The sum over the states i was rewritten using the standard expression for the Green function at energy E:

$$G(x,z;x',z';E)=\lim_{\epsilon\to 0}\sum_i \frac{\psi_i(x,z)\psi_i^*(x',z')}{E-E_i+i\epsilon} .$$

In order to get the semiclassical current the Green function was replaced by its semiclassical form expressed as a sum over classical trajectories cl going from $(\bar{x},z)$ to $(\bar{x},z')$. Neglecting incoherent processes and overall factors due to reflections against the barriers, one obtains

$$I(E)\propto \mathrm{Re}\sum_{cl}\int dz\int dz' m_{12}^{-1/2} e^{iS(z,z')} e^{-B\cos\theta(z^2+z'^2)/2},$$

where $m_{12}=\partial z/\partial p_{z_0}$. To evaluate the integrals, further stationary phase approximations are needed. In [16] it was concluded that the stationary phase conditions are $\partial S/\partial z=\partial S/\partial z'=0$, which imply that only orbits with initial $p_{z_0}=0$ contribute to the current. These orbits must be periodic orbits or in special cases segments of periodic orbits. This is one respect in which this theory deviates substantially from the Gutzwiller trace formula, since in that case stationary phase implies $\partial S/\partial z-\partial S/\partial z'=0$, which includes all periodic orbits rather than just a small subset.

Finally, in order to simplify the integrals, it is assumed that

$$\left|\frac{\partial^2 S}{\partial z_0^{\,2}}\right| \gg B.$$

In that case, the stability prefactor is found to have a simple analytic form: $|m_{21}|^{-1/2}$, where $m_{21}=\partial p_z/\partial z_0$ is an off-diagonal element of the stability matrix. This is also quite different from the Gutzwiller trace formula, where the trace integral yields $|\det(M-I)|^{-1/2}$.

Note that the tunneling through the second barrier affects the relative PO amplitudes weakly, though it has a strong effect on the global tunneling envelope $G(E)$. For the quantal and experimental currents, we evaluated the effects from the $I(V)$ traces at $\theta=0°$ as described in Sec. III. The global envelope $G(E)$ was eliminated from our semiclassical, experimental, and quantal results. The incoherent processes produce simply an exponential damping term $\sim\exp(-\kappa T)$ for a PO with period T. Their effect is essentially to cut off the contribution from longer orbits. Experimentally, only period doubling or tripling is seen, which suggests that only POs with $T<4T_0$ contribute, where T_0 is the period of the main t_0 orbit.

In order to exploit fully the scaling property of the RTD, we first write

$$S=B\tilde{S}(\epsilon)=2\pi N\hat{S}(\epsilon).$$

Here $\hat{S}=\tilde{S}/\tilde{S}_0$, $\tilde{S}_0$ is the approximate scaled action of t_0 for $\theta=0°$ and the scaled magnetic field N, defined in Sec. II, gives roughly the number of oscillations of the wave function along the x dimension. We define also $N_L=mL(\mathcal{R}+1/2)B\epsilon$ associated with the quantization along z; N_L gives approximately the number of Landau states supported by the well. Both N and N_L are a measure of effective $\hbar^{-1}$; N_L determines the size of classical invariant phase-space structures on the surface of section relative to an $\hbar$ cell and hence is important in determining whether periodic orbits may be considered isolated.

Finally we write the current as a function of N instead of E. The final expression is

$$I(N)=\text{const}\times\sum_{p,j} A_j^{\text{SC}}\cos 2\pi[jN\hat{S}-\mu(j)/2], \qquad (2)$$

$$A_j^{\text{SC}}=\frac{|\phi_0(z_0)|^2}{|m_{21}(j)|^{1/2}},$$

where $\hat{S}$, μ, and z_0 are, respectively, the scaled action, the Maslov index, and the initial position of a primitive PO p, and j denotes its repetitions. We shall consider that the initial state in the 2DEG is described by the lowest Landau level:

$$\phi_0(z_0)=\frac{\alpha^{1/2}}{\pi^{1/4}}e^{-z_0^2\alpha^2/2}\ , \quad \alpha=\sqrt{B\cos\theta}\ . \qquad (3)$$

In scaled coordinates, the model is valid if

$$\left|\frac{\partial^2\widetilde{S}}{\partial {z_0}^2}\right|\gg 1\ .$$

We discuss the validity of this assumption in Sec. VII.

In Sec. VII we compare A_j^{SC} with A_j^{QM}. The point here is that a Fourier transform of $I(N)$ with respect to N, done over a finite N range, would have peaks whenever $\hat{S}'=j\hat{S}$, with an amplitude A_j^{SC}. In this way, we are able to identify and compare contributions from primitive POs as well as their repetitions. Period-one oscillations of $I(V)$ are due to POs with $\hat{S}\simeq 1$, while period-two oscillations are due to either the first repetition of a PO with $\hat{S}\simeq 2$, or the second traversal of a PO with $\hat{S}\simeq 1$.

V. CLASSICAL STABILITY ANALYSIS OF *T* AND *S* ORBITS

The objective here was not to carry out an exhaustive study of the classical dynamics, which may be found in [7]. We concentrated on the few short POs that can be resolved experimentally.

The stability of each individual PO is determined by its stability (monodromy) matrix M. This matrix is obtained by investigating the linearized classical dynamics in the neighborhood of the PO. More precisely, we define a slice of phase space [a Poincare surface of section (SOS)] perpendicular to the PO. We consider a small initial displacement $\boldsymbol{\delta\mu_0}$ from the PO on the SOS. The next intersection of the perturbed trajectory with the SOS defines a new displacement $\boldsymbol{\delta\mu}_1$ from the PO. M is given simply by the linearized relation between the two displacements:

$$\boldsymbol{\delta\mu}_1=M\,\boldsymbol{\delta\mu}_0.$$

Details are given in the Appendix. For a stable orbit, the eigenvalues of M are complex quantities $\exp(i2\pi\nu)$, and define the winding number ν of the periodic orbit. For an unstable orbit of period T, the largest eigenvalue $\exp(\lambda T)$ defines the Liapunov exponent λ.

An orbit destabilizes when

$$|\text{Tr}M|=2.$$

A synchronous bifurcation occurs for $\text{Tr}M=2$ and a period-doubling bifurcation occurs for $\text{Tr}M=-2$. At these points, the semiclassical density of states (as given by the Gutzwiller trace formula) diverges. Whether the semiclassical current itself diverges depends on the form of its weighting. The semiclassical theory proposed by [16] diverges at points where $m_{21}=0$. Although the quantum current does not become infinite (these divergences can be removed by use of uniform approximations), one might still expect the current amplitude to be enhanced substantially at a semiclassical divergence. But the important point is that not all bifurcation points $|\text{Tr}M|=2$ coincide with divergences of the current, i.e., $m_{21}=0$ in this model. Conversely, not all $m_{21}=0$ points are bifurcations. For example, we have found two points (at $\theta=11°$, $\epsilon=1350$ and 7050), which should diverge for the second repetition of t_0 since $m_{21}(2t_0)=0$. This occurs wherever $\text{Tr}M(t_0)=0$, since $m_{21}(2t_0)=m_{21}(t_0)\text{Tr}M(t_0)=0$.

The experimental behavior in [2] is dominated by the main 2-bounce periodic orbits (t_0 and t_2), responsible for the period-one oscillations, and the 3-bounce orbits (S_1 at 11° or S' at $\theta=27°$) for the period-two oscillations, so we have focused our detailed stability analysis on these four important periodic orbits. Their shape in the x-z plane is shown in Fig. 3(a).

In Fig. 3(b) we plotted the classical Poincaré surface of section for $\theta=27°$ taken on the emitter wall: $\{x=0,p_x>0\}$. The equivalent SOS for $\theta=11°$ were shown in [6]. The figure illustrates the fact that the classical dynamics, for given θ, evolve from regularity to chaos with *decreasing* ϵ.

We see that for high $\epsilon>17\,000$ there is a large island of stability centered on the main and shortest 2-bounce orbit t_0. It undergoes two successive period-doubling bifurcations and is unstable between them for $\epsilon\simeq 13\,000$. The same happens at $\theta=11°$. The stability island of t_0 shrinks gradually and disappears in a tangent bifurcation leaving a ''chaotic sea'' of unstable POs. Another prominent feature in Fig. 3(b) is the central stable island associated with the 3-bounce PO S', which is born stable ($\epsilon=18\,050$), loses its stability ($\epsilon=13\,650$), and disappears in a tangent bifurcation ($\epsilon=7750$).

The second important factor that determines whether an orbit is experimentally visible is its accessibility. A necessary condition for a PO to be accessible is that its starting point, the initial z_0, corresponds to a non-negligible probability density of the initial state so

$$|\phi_0(z_0)|^2\sim e^{-z_0^2B\cos\theta}$$

should not be small. Neglecting the shift between the edge of the 2DEG and $x=0$ (a reasonable assumption for θ not too large) the smaller z_0 is the more accessible the PO. An important feature to notice is that although the classical stability does not depend on B for fixed ϵ, the accessibility does, i.e., it may be said to be $\hbar$ dependent. Two weightings corresponding to $B=1$ T and $B=6$ T are plotted in the SOS for $\epsilon=20\,000$ in Fig. 3(b). This B dependence of the weighting has interesting consequences in the regular torus quantization regime as we will show in Sec. VIII.

In Fig. 4 we can examine the relative importance of the stability versus accessibility factors by comparing the trace of the stability matrix $\text{Tr}M$ with the initial position z_0 for the

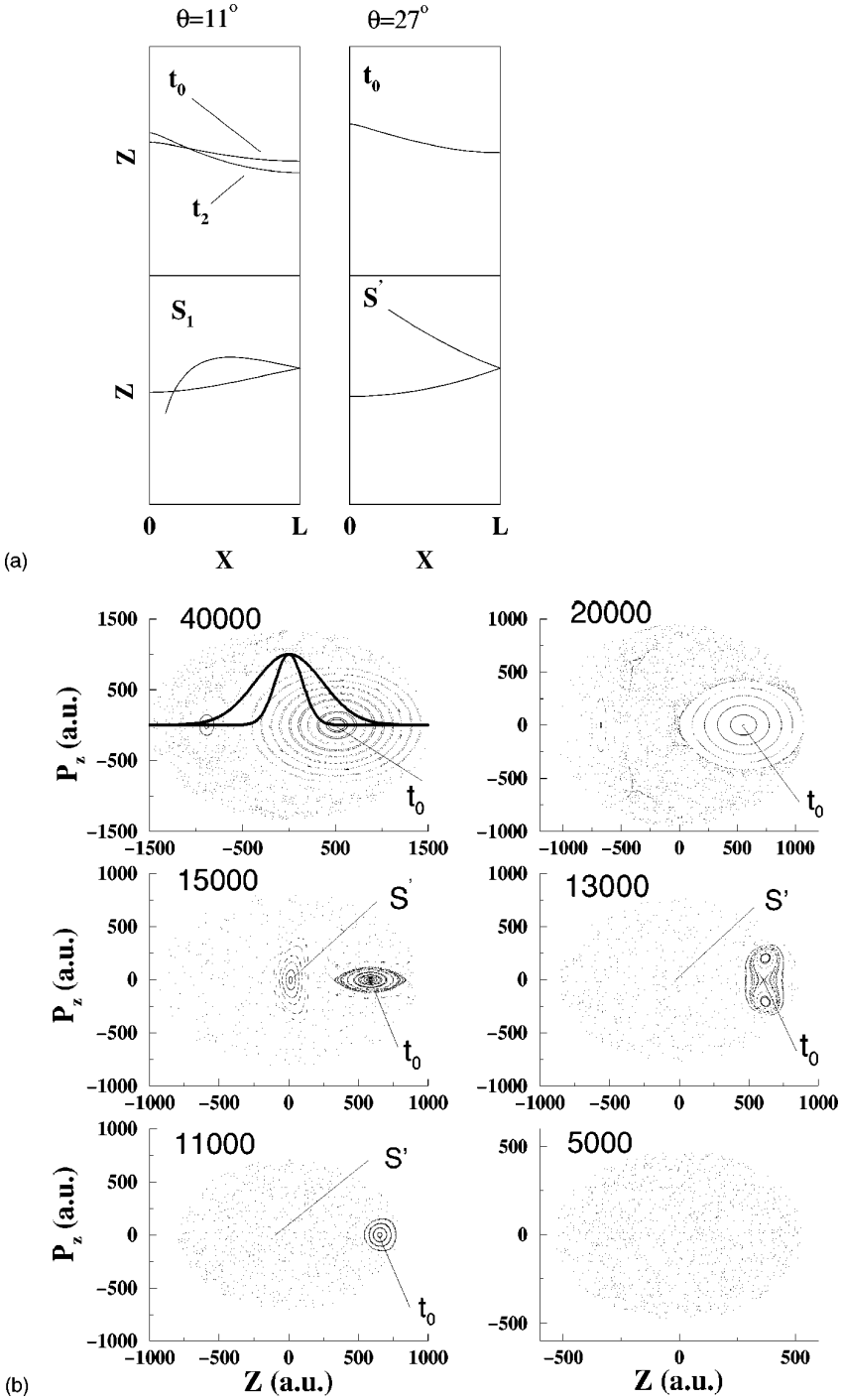

FIG. 3. (a) Main periodic orbits which dominate the current oscillations at $\theta=11°$ and $\theta=27°$. t_0 gives the main period-one current. t_2 is an unstable PO, which coalesces with t_0 in a series of tangent bifurcations. S_1 and S' are 3-bounce orbits responsible for some of the period-doubling regions. (b) Poincare surfaces of section for $\theta=27°$ for different values of $\epsilon=F/B^2$. The dynamics becomes progressively more chaotic as ϵ decreases.

main orbits. $\theta=11°$ is shown in Fig. 4(a) and $\theta=27°$ in Fig. 4(b) for the t and S orbits. In the TrM plots, we indicate with an arrow where $m_{21}=0$.

At $\theta=11°$ we see from TrM that t_0 undergoes an ''infinite'' sequence of bifurcations alternating between period-doubling (Tr$M=-2$) and tangent (Tr$M=2$) bifurcations. An analysis of the infinite sequence was given in [7]. The plots of z_0 illustrate clearly the sequence of tangent bifurcations and one can identify ranges of ϵ where no real 2-bounce (period-one) orbit exists, principally below $\epsilon=6500$. We see that the first period-doubling seen experimentally (PD1) is related to the double pitchfork bifurcation of t_0 around $\epsilon=13\,000$. The orbit crosses twice the Tr$M=-2$ line, when it destabilizes ($\epsilon=12\,800$) and restabilizes ($\epsilon=13\,100$). However, only the latter bifurcation has $m_{21}=0$.

TrM for the S_1 PO exhibits approximately a ''saddle'' shape around $\epsilon=3000$, which corresponds to PD2. We refer to this feature as a ''failed bifurcation'': for a small increase in the energy-voltage ratio $\mathcal{R}$ from 0.15 to 0.20, this saddle turns into an actual double bifurcation. In that case, we would get $m_{21}=0$ for two consecutive ϵ, and related divergences in the semiclassical current. Also, z_0 is small and the accessibility is favorable. A reduction in $\mathcal{R}$ on the other hand would remove the saddle and hence weaken the period-doubling feature due to S_1. The dotted line shows the orbit born with S_1 at the tangent bifurcation ($\epsilon=2100$). With increasing ϵ, this other orbit stabilizes and destabilizes very quickly so its contribution is negligible.

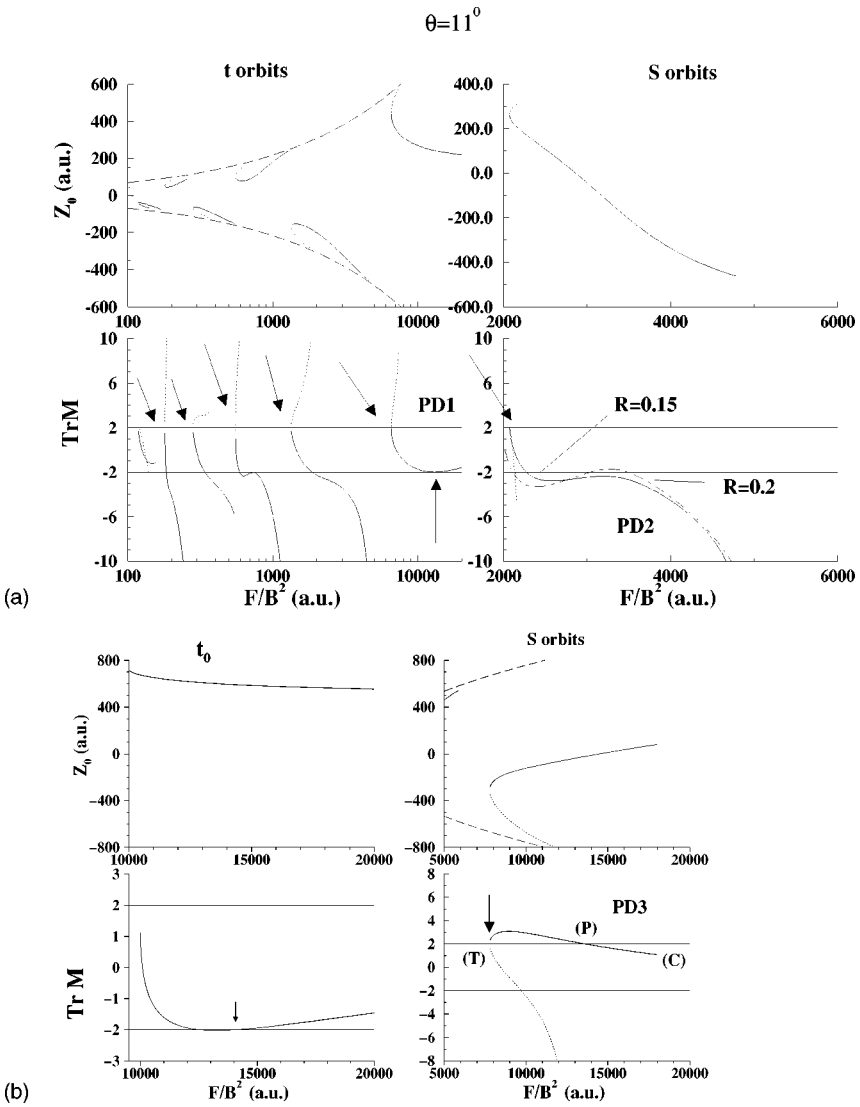

FIG. 4. Evolution of classical properties of the main POs with ϵ. z_0 indicates the starting position on the SOS, and the limits of the SOS are shown (long-dashed lines). All these orbits start with $p_{z_0}=0$. TrM indicates the trace of the stability matrix. Synchronous (Tr$M=2$) and period doubling (Tr$M=-2$) bifurcations are shown by the thin horizontal lines. PD indicates a region corresponding to a significant experimental period doubling. The arrows indicate where $m_{21}=0$. (a) $\theta=11°$. For t orbits, the z_0 plot shows the infinite set of tangent bifurcations involving t_0 (stable, solid line) and t_2 (unstable, dotted line). The stability shows alternating period-doubling and tangent bifurcations. PD1 corresponds to a 2-resonance of the period-one orbit t_0. For S orbits, PD2 corresponds to the ''failed'' bifurcation of S_1: a small increase in injection energy to $\mathcal{R}=0.2$ brings about an actual period-doubling bifurcation (dashed line). S_1 stabilizes and then disappears in a tangent bifurcation with another orbit (dotted line) at $\epsilon=2100$. (b) $\theta=27°$. The z_0 of t_0 remains high throughout the experimental range, which covers PD3. For S', we have a set of three bifurcations [pitchfork (P), cusp (C), and tangent (T)]. Only the T bifurcation has $m_{21}=0$.

At $\theta=27°$ we see that the 3-bounce orbit S' undergoes two bifurcations where Tr$M=2$: a tangent bifurcation at $\epsilon=7750$ (T) and a pitchfork bifurcation at $\epsilon=13\,650$ (P). In addition it appears at $\epsilon=18\,050$ with Tr$M=1.07$ (C). This has been termed a ''cusp-bifurcation'' by [7] (who found many other examples in this problem) and is a nongeneric type of bifurcation due to the nonanalytic character of potential. Over all this range, which corresponds to PD3, z_0 is not too large. The period-doubling bifurcation of t_0 occurring around 13 000 is shown, where again, as for $\theta=11°$, m_{21} goes to 0. However, the accessibility is very low since z_0 is large.

We have identified many bifurcations, so the question remains: why are only a few singled out as experimental period doublings? Provided an orbit is reasonably accessible, the important characteristic is that the amplitude should stay large over a significant interval of V/B^2 (i.e., covering several I-V oscillations). Only then can an enhanced amplitude be resolved experimentally. In the present model this corresponds to m_{21} being small (not necessarily zero). Hence we find that the important requirement is a low slope of m_{21} in a region where m_{21} is small (not necessarily zero) over a broad parameter range. In general it also correlates with the orbit being near stable $|\mathrm{Tr}M|\sim 2$. It excludes divergences such as those at $\epsilon=1350$ and 7050 or found near the tangent bifurcations, which are much narrower than a single I-V oscillation.

This factor is common to regions PD1, PD2, and PD3, which otherwise have different dynamical origins: PD1 is a double-pitchfork bifurcation of t_0, PD2 is an isolated unstable orbit (albeit a ''failed'' bifurcation), and PD3 is a set of three consecutive bifurcations (cusp, pitchfork, and tangent) of the orbit S'. Their effects all persist over a wide parameter range.

VI. EXPERIMENTAL ANALYSIS

In Sec. III we described our procedure for extracting the pure periodic orbit spectrum from the experimental data, by subtracting the smooth term and normalizing to the $\theta=0°$ tunneling envelope.

The resulting reduced experimental spectra for $\theta=11°$ are shown in Fig. 5(a). We indicate in the experimental figure three parabolas of constant $\epsilon=19\,000$, 6500, and 3000. The arrows indicate the $\hbar\to 0$ limit. The figure illustrates how the typical line profiles evolve with ϵ and gives an indication of the validity of the scaling. Four distinct regions stand out:

(1) A pure period-one region above the $\epsilon=19\,000$ pa-

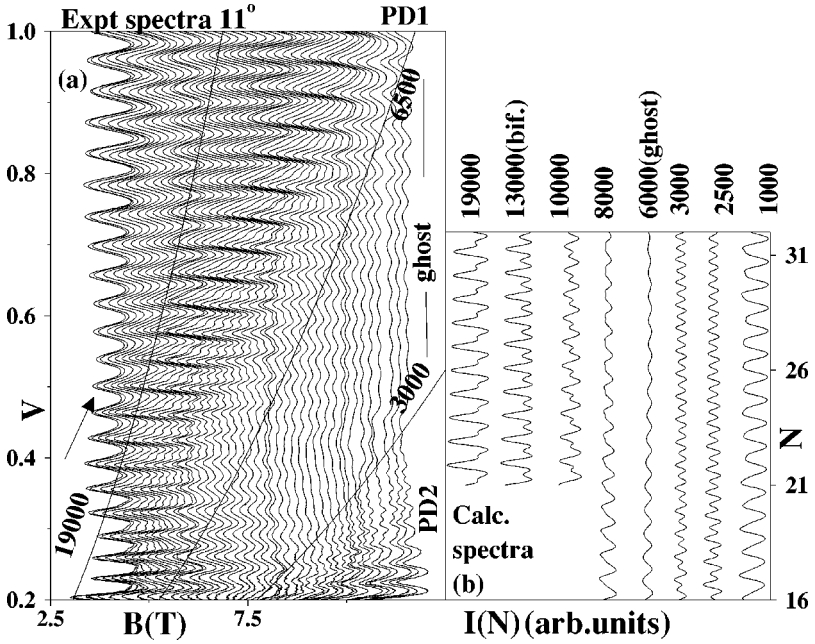

FIG. 5. Comparison between experimental and theoretical line profiles at $\theta = 11^o$ showing effects of approximate scaling dynamics. (a) Experiment: set of I-V traces (reduced current) showing characteristic line profiles roughly along parabolas of constant $\epsilon = F/B^2$. The period-doubling regions PD1 and PD2 are shown along with the ''ghost'' region where the results are not due to a real PO. The arrows indicate the semiclassical limit. (b) Theory: smoothed theoretical spectra. The quantum number N is proportional to magnetic field B. The range $N = 12-42$ corresponds to voltage range $0.1-1.1$ V. With decreasing ϵ, right asymmetric profiles ($\sim 19\,000$) evolve into symmetric period-doubled profiles at the bifurcation. Below the tangent bifurcation (~ 6500) the ''ghost'' has a weak sinusoidal profile. PD2 is mainly due to S_1 but has substantial period one interference, indicating that t_0 is still accessible.

rabola. (2) The PD1 period-doubling region. Here we see that the line profiles evolve systematically from right-asymmetric, to symmetric, to left-asymmetric with decreasing ϵ. (3) The region roughly in between the $\epsilon = 6500$ and 3000 parabolas (i.e., in between PD1 and PD2) showing a striking drop in the amplitude of the period-one modulations. There is also a rapid fall in amplitude with decreasing effective $\hbar$. We attribute this region to a ''ghost'' contribution [18]. It results from a tangent bifurcation at $\epsilon \simeq 6500$, which eliminates t_0. (4) The PD2 period-doubling region is quite narrow and clearly shows interference with a period-one contribution (partly from the ghost and partly from the reappearance of t_0).

We emphasize that the striking ''valley'' in the amplitude due to the ghost appears only with our analysis, which removes $G(E)$, the tunneling envelope. $G(E)$ increases rapidly and monotonically with voltage and hence masks the underlying PO behavior, which in the ghost region decays with decreasing $\hbar$.

In [6] we compared individual quantal and experimental I-V traces. Here we wish, instead, to systematically compare our theoretical scaled quantum spectra with the experimental line profiles along curves of constant ϵ. The objective is to show that we can follow the locus of constant ϵ in the experiment, although the parabolas are a little distorted and displaced.

We show in Fig. 5(b) smoothed quantum line profiles obtained in [6] along curves of constant ϵ at 11°. The theoretical spectra show characteristic line profiles, which are in excellent agreement with the experimental profiles, albeit somewhat displaced. For the first period doubling (PD1) at $\epsilon \simeq 19\,000-10\,000$, the change from a right-asymmetric to a left-asymmetric profile confirms the analysis in [6]. The period-doubling bifurcation coincides with the symmetric profile. In the experiment, it appears along an approximately linear locus close to $\epsilon = 10\,000$, instead of the parabola $\epsilon = 13\,000$ predicted by the classical dynamics and seen on the quantum lines.

Figure 5(a) also confirms how the high voltage cutoff of PD1 is largely due to the increase in line broadening with voltage due to coupling with the continuum. With increasing voltage the period-doubling peak turns into a ''shoulder'' and finally is absorbed by the main peak.

For the PD2 region at $\epsilon < 3000$ the characteristic line profiles change rapidly with ϵ since they result from the interference between a period-one (t_0) and two separate period-two contributions ($2t_0$ and S_1) with rapidly varying amplitudes. Nevertheless one can identify typical profile shapes over narrow ranges.

In both quantum and experimental spectra near 6000 we see a period-one region with simple sinusoidal profiles which decay rapidly with decreasing $\hbar$. The sinusoidal profile is expected from a ghost, since it has negligible harmonics. Although a period-one orbit does reappear near 4000 its contribution is weak as will be shown in Fig. 7(a) below. The quantum Fourier transform peak near period-one only corresponds to the action of the real orbit below 3000.

Figure 6 shows the equivalent picture for $\theta = 27°$. The period-doubling region PD3 dominates these experiments. The most striking aspect of that region is that despite four bifurcations being involved (three for S' and one for $2t_0$) PD3 appears as a broad, flat ''plateau'' of period-two oscillations. There is absolutely no evidence of a strong maximum that one might associate with a divergence in the semiclassical current. Unsurprisingly, the scaled quantum spectra (not shown here) produce a pure period-two oscillation over a range approximately equivalent to PD3.

VII. RESULTS: QUANTUM AMPLITUDES VERSUS SEMICLASSICAL AMPLITUDES

We evaluated the semiclassical amplitudes (A_p^{SC}) as a function of ϵ for the main POs t_0, S_1, and S', taking only the first or second repetition. The 2-bounce periodic orbit t_0 contributes to a period-one current, while its second repetition $2t_0$, as well as the 3-bounce POs S_1 and S', contribute to the period-two current. We compared the values of A^{SC} with the quantum A^{QM} within the experimental range of ϵ.

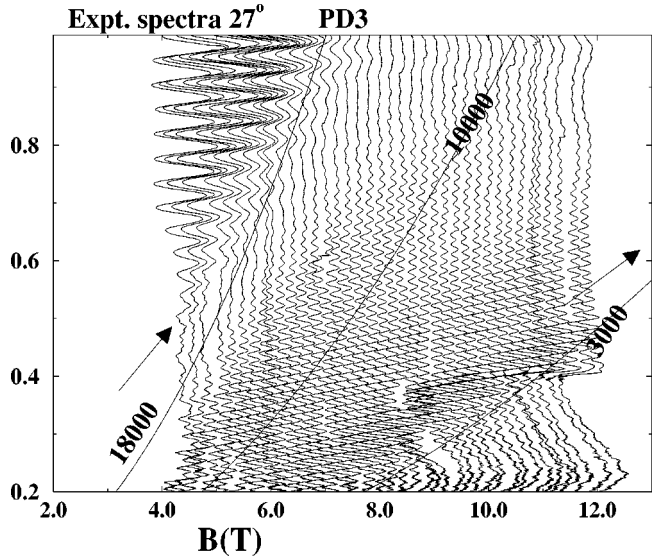

FIG. 6. Experimental traces at $\theta=27°$ showing the broad ''plateau'' of period-doubled current corresponding closely to the range of the quantum maximum shown in Fig. 7(c) rather than the range of the semiclassical current. This indicates that contribution is not due to real PO over about half the experimental period-doubled range (below $\epsilon\sim 8000$ and above $\epsilon\sim 18\,000$).

We have investigated thoroughly the condition $|\partial^2\widetilde{S}/\partial {z_0}^2|\gg 1$ on which the semiclassical expression depends. We found that, unfortunately, throughout much of the experimental range we investigated, $|\partial^2\widetilde{S}/\partial {z_0}^2|\sim 1$. The validity of the assumption is especially poor over the regular (high ϵ) regime. It is reasonably satisfied ($|\partial^2\widetilde{S}/\partial {z_0}^2|\sim 10$) for t_0 near $\epsilon\sim 2000$.

All our calculated amplitudes are relative, so they must be normalized. In the experimental and quantum case we normalize our results to the period-one amplitude at $\theta=0°$ since this is a pure period-one region. The experimental amplitudes were estimated by reading directly the peak heights of the normalized spectra at applied voltage $V\simeq 0.52$ V in Fig. 5(a), the peaks which (assuming $V\sim FL$) correspond most closely to $N\sim 1/27$. The semiclassical expression has no good $\theta=0°$ limit, so the A^{SC} were normalized by equating the quantal and semiclassical period-one current at the point $\epsilon=1900$, where the expression is most valid.

The results are shown in Fig. 7. In general, we see that the agreement between the quantal and semiclassical currents is qualitative at best.

Figure 7(a) shows the period-one current for $\theta=11°$. The quantitative agreement between the quantal calculation and the experimental results is reasonable given the uncertainty in V. So is the comparison between A^{SC} and A^{QM} for the region $\epsilon<3000$.

A major disagreement appears in the region between $\epsilon=3000$ and $\epsilon=6500$ where there is significant experimental and quantal period-one current but no significant semiclassical current. As this gap appears below the tangent bifurcation which removes t_0, we suggest that a ''ghost'' complex PO is responsible for the current. However, a simple cubic normal form treatment suggests that the ghost contribution would decay too quickly to account for the very wide experimental region seen in Fig. 5(a). One possible explanation is that the complex part of the action of the ghost remains small throughout. Testing this hypothesis will require an investigation of the complex classical dynamics. The agreement between quantal and semiclassical current is very poor for $\epsilon>7000$ where t_0 has a large stable island. In fact it worsens

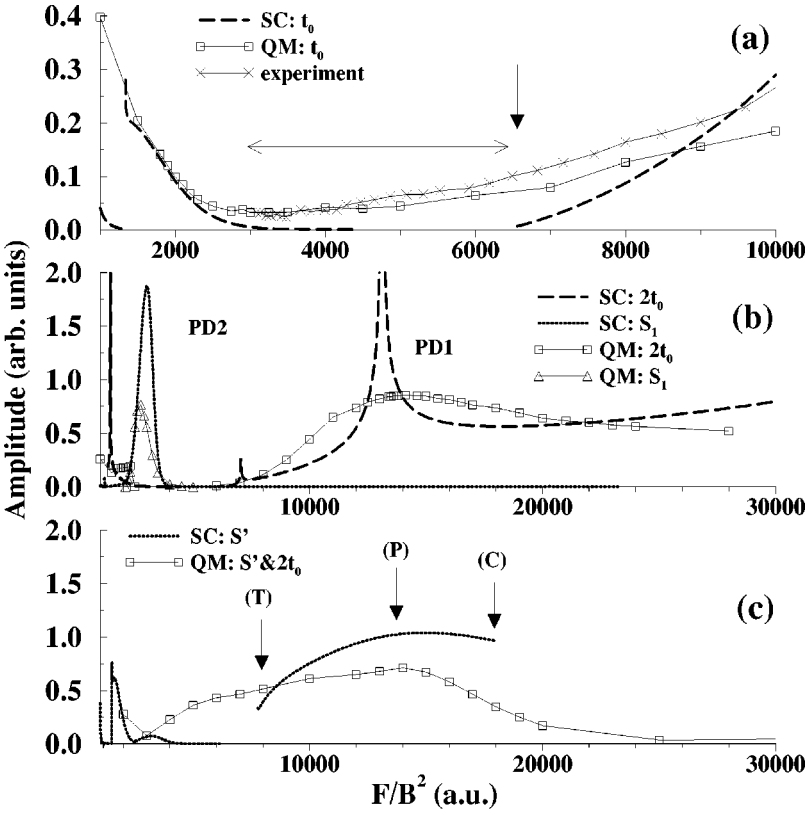

FIG. 7. Comparison between quantum (QM), periodic orbit theory (SC), and experimental amplitudes for period-one and period-two current. The vertical arrows indicate the position of important bifurcations. (a) Period-one current at $\theta=11°$. The arrow indicates the tangent bifurcation, which removes the period-one orbit t_0. Down to $\epsilon=3000$ (the ''ghost'' region marked by a horizontal arrow) there is no significant contribution from a real PO that can account for the quantum or experimental results. Where there is a large stability island ($\epsilon>7000$), the semiclassical formula breaks down completely. (b) Period-two current at $\theta=11°$. PD2 is due to the ''failed'' bifurcation of S_1, while PD1 coincides with the double pitchfork bifurcation of t_0. Two divergences of PO theory for $2t_0$ at $\epsilon=1450$ and $\epsilon=7050$, where $m_{21}=0$, are not seen in the QM calculation. (c) Period-two current at $\theta=27°$. The large region PD3 is largely due to S', as the accessibility of t_0 is very low for $\epsilon<16\,000$. Again, there are two regions ($\epsilon<8000$ and $\epsilon>18\,000$) where there is a quantal current, but no contributing PO. The arrows indicate the three bifurcations of S', cusp (C), pitchfork (P), tangent (T).

with increasing ϵ. We shall investigate large islands of stability in Sec. VIII.

In Fig. 7(b) the period-two current for $\theta=11°$ is shown. We see that PD2 is due to the ''failed'' bifurcation of S_1. PD1, on the other hand, is associated with the double pitchfork bifurcation of t_0. Narrow semiclassical divergences of $2t_0$ occur at $\epsilon=1450$ and $\epsilon=7050$, where $m_{21}=0$. These are not associated with bifurcations, and are not seen in the QM calculation. The tangent bifurcations of t_0 at $\epsilon=1350$ and 6550 also give rise to divergences in both period-one and -two current, which do not manifest themselves in the QM spectra. This suggests that narrow divergences are not detectable for such large $\hbar$.

Figure 7(c) shows the period-two current for $\theta=27°$. The quantal amplitudes are consistent with the wide experimental period-two plateau of PD3 seen in Fig. 6. However, the period-two orbits are suppressed relative to the period-one orbits by a factor $\sim\exp(-\kappa T_0)$ by incoherent processes and additionally by coupling to the continuum. We estimate that the peak period-doubled experimental amplitudes are ~ 12 times weaker than the peak quantum equivalent at $V\sim 0.5$ V. Because of this added uncertainty we have not carried out a detailed quantitative analysis of the experiment here.

PD3 is almost entirely due to S' or its ghosts, as the accessibility of t_0 is too unfavorable. The semiclassical contribution of $2t_0$ to the period-two current is much less than 1% of S' near 13 000. However, once again we find that nearly half of the period-two region corresponds to a ghost. There are two regions ($\epsilon<7750$ and $\epsilon>18\,000$) where there is a quantal current, but no contributing PO, as S' disappears in a tangent (T) or cusp (C) bifurcation, respectively. In particular the cusp bifurcation at $\epsilon=18\,000$ is an interesting feature, as S' does not disappear through a generic bifurcation [$\mathrm{Tr}(M)=1.076$ rather than $|\mathrm{Tr}(M)|=2$], but because one of its legs reaches a discontinuity. This occurs where a turning point on the energy surface turns into a specular bounce against the emitter wall. The other leg of the orbit strikes the central region and remains highly accessible to the tunneling electrons. Diffractive corrections to the PO theory may become important here.

We do not show the period-one currents for $\theta=27°$. The only significant contribution occurs when there is a large stable island and here the semiclassical model gives poor results.

We now discuss the limitations of the semiclassical model. Clearly any basic semiclassical model will fail in ghost regions and divergences since we have not included normal forms or complex orbits. The semiclassical model fails for large ϵ, in the regular regime and we investigate this case in the next section.

Another cause for uncertainty is the moderate value of effective $\hbar$ considered since $N\sim 27$. In comparable atomic systems excellent quantitative agreement is obtained with semiclassical theories only for somewhat smaller values of $\hbar\sim 1/100$.

However, here we find that the main problem with the model derives from the assumption that $|\partial^2\tilde{S}/\partial z_0{}^2|\gg 1$. We have investigated this condition numerically and find that it is not at all valid in the stable regime. It is weakly satisfied for low ϵ hence the moderate agreement shown in Fig. 7(a) and 7(b) for $\epsilon<3000$.

Interestingly, close to the synchronous bifurcation in Fig. 7(c) at 27° the Gutzwiller formula has a very large strong divergence, of which there is no sign in the amplitude ''plateau'' seen in both experiment and quantal currents. Hence the semiclassical model here, which has no divergence either, does provide useful insight into the differences between the behavior of the current and the density of states.

VIII. TORUS QUANTIZATION

The aim of this section is to understand the semiclassical current in the RTD for a stable PO surrounded by a large stable island. We know from Miller [19] that for such a PO the sum over repetitions appearing in the Gutzwiller density of states will resolve discrete states: they are series of harmonic oscillatorlike levels with quantization condition [19] $S=2\pi\hbar[m+(K+1/2)\nu+\mu/4]$, where m represents quantization along the orbit and K perpendicular to the orbit. That harmonic approximation yields quantum states localized on tori around the central PO.

Equation (2) in effect attributes the same accessibility to all the tori. Clearly outer tori of the island have a different accessibility from the state localized on the central fixed point. Therefore we build the semiclassical current from a sum of tori with different weighting:

$$I(N)=\sum_{K,m} W_K\delta\left(N-\frac{1}{\hat{S}}[m+(K+1/2)\nu+\mu/4]\right)$$

for a stable PO with rescaled action $\hat{S}$ and winding number ν. The B-dependent weighting W_K for the Kth torus is the overlap in z_0 between the injection state given by Eq. (3) and the torus state. The latter is a harmonic oscillator (HO) in the Kth state with HO constant $\beta=\sqrt{\sin(2\pi\nu)/m_{12}}$. We easily get

$$W_K(1)=\frac{\alpha\beta|\alpha^2-\beta^2|^2}{2^{K-1}K!(\alpha^2+\beta^2)^2}e^{-(\alpha^2\beta^2/\alpha^2+\beta^2)z_0^2}\times\left|H_K\left(-z_0\frac{\alpha^2\beta}{\sqrt{|\beta^4-\alpha^4|}}\right)\right|^2. \quad (4)$$

We note that in the integrable limit (i.e., $\epsilon\to\infty$ or $\theta\to 0°$) we have $\beta\to\alpha=\sqrt{B\cos\theta}$. In that case, the torus states reduce simply to displaced Landau states, centered on z_0 rather than $z=0$. With that approximation, one gets

$$W_K(2)=\frac{1}{K!}\left(\frac{\alpha^2 z_0^2}{2}\right)^K e^{-\alpha^2 z_0^2/2}. \quad (5)$$

In Fig. 8 we show a comparison between the quantum spectrum and the tori expression (4) for $\epsilon=20\,000,\theta=27°$. We see that the modified expression gives very good agreement over the experimental range using a set of 8 tori $K=0,1,\ldots,7$. For each K, the torus series in m in effect represents a period-one series, dephased from the next series by an amount proportional to ν. As B is increased the tunneling electrons scan different parts of the island selecting preferentially higher K (i.e., the outer tori). Depending on the ex-

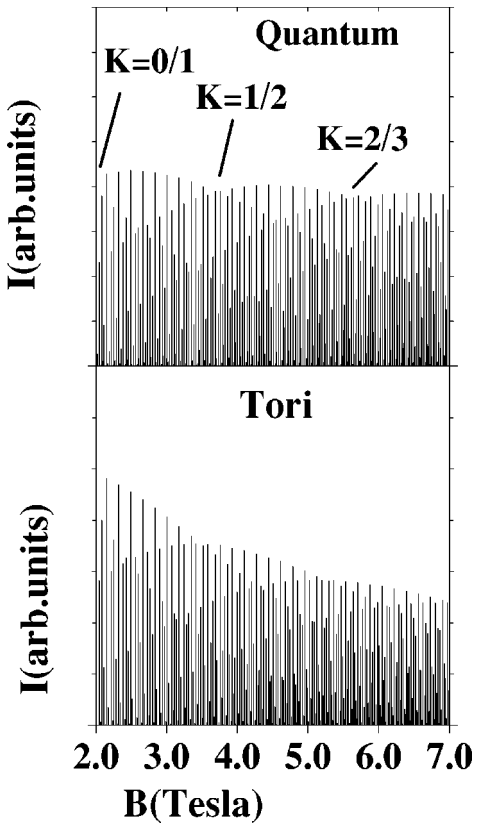

FIG. 8. Spectra for $\epsilon = 20\,000$ at $\theta = 27°$ in the torus quantization regime. The semiclassical spectra are weighted by a K-dependent weighting using a harmonic approximation about the elliptic fixed point of t_0. The Gaussian ''envelopes,'' reflecting the variable accessibility of the different tori, are clearly seen. The regions where the dominant torus changes are indicated.

perimental resolution relative to ν (i.e., the displacement between tori) one can sometimes observe two torus series simultaneously. In particular at the changeover between two torus series they are equally favored by the tunneling electrons. For $\beta \simeq \alpha$, this occurs at

$$B \simeq \frac{2(K+1)}{z_0^2 \cos\theta} \ .$$

At 27°, $z_0 \simeq 500$ for all ϵ hence the $K = 0/1$ changeover occurs at $B \simeq 2$ T, the $K = 1/2$ changeover occurs at $B \simeq 4$ T. The voltage range $V = 0.5$ V is most favorable in terms of resolution. In Fig. 1 we see two ''jumps'' in current for 27° near 2 and 4 T corresponding to the band where a $(K+1)$th series takes over from the Kth one. These features are seen for all experiments in the $14-31°$ range. At 11° the island is more central so only the $K = 0/1$ changeover is visible. In fact it is less obvious since it occurs within the large period-doubling region PD1. There the period-doubling bifurcation corresponds to $K = 0$ and $K = 1$ series, which are exactly π out of phase since $\nu = 1/2$.

In [20] it was argued that the signature of a stable island in this system is seen as broad period-one resonances. In fact it consists of discrete states spaced exactly by $1/\hat{S}$ of t_0 for a given K series. In [20] states supported by the island were equated with the original in-plane Landau states and so would be inaccessible due to conservation of in-plane Landau quantum number. But the large displacement of the island ensures that this is not the case. In [20] the sudden broadening of the oscillations, which were attributed to the large island appears even for 0° so they may be due to coupling with the continuum or some other cause.

The large stable islands also support states mainly localized on outer ''broken-tori'' lying just beyond the confines of a large stable island, in a regime where the harmonic approximation should give poor results. We have generated semiclassical torus spectra like Fig. 8, including one or two tori just beyond the edge of the island, then Fourier transformed them to obtain new amplitudes to be compared with the quantum results.

A comparison between the amplitudes of the tori and the quantum results is shown in Fig. 9. The agreement with QM amplitudes is excellent for both Eqs. (4) and (5). At the bifurcation near $\epsilon = 13\,000$, Eq. (5) remains smooth whereas Eq. (4) diverges. For these values of $\hbar$ the region PD1 is almost completely due to ''dephasing'' of torus states, with no detectable contribution from the stable-unstable pair of orbits born at the bifurcation. A substantial part of the improved agreement is due to the wider torus envelope $\sim \exp[-(Bz_0^2 \cos\theta/2]$ whereas the isolated PO expression is weighted by the narrower function $\sim \exp[-(Bz_0^2 \cos\theta)]$.

The agreement in Fig. 9(d) is surprising: the rise in period-doubled current at 27° in the range $20\,000 - 16\,000$ is extremely well described by the tori of the t_0 island. Yet this region was apparently dominated by the cusp-bifurcation orbit S' [see Fig. 7 (c)]. This provides a striking illustration of the fact that this system so frequently defies description in terms of isolated periodic orbits. It suggests that the amplitude due to orbit S' down to about 16 000 appears within ''quasitori'' beyond the edge of the t_0 island.

IX. SUMMARY AND CONCLUSIONS

This work underlines the interest of the RTD, not only as a probe of periodic orbit effects in a semiconductor device but also as a probe of effects not due to real isolated periodic orbits (bifurcations, complex orbits, tori, and broken tori, possibly diffractive orbits).

We have calculated a set of reduced experimental spectra that isolated the PO contributions to the current. In this way we were able to expose graphically features such as the ghost region at 11°. We calculated a set of accurate quantum current amplitudes, extending considerably the calculations in [6]. These normalized amplitudes may be used to test improvements to the semiclassical theory.

We have tested the validity of the scaling by comparing experimental and quantal line profiles along constant V/B^2 curves. Previously we had only considered amplitudes in individual I-V traces. The results demonstrate that the experimental line profiles do remain roughly constant along slightly distorted and displaced parabolas. Hence the scaling analysis is a useful technique in many experimental regimes. We conclude that three major factors affect the V/B^2 invariance: (1) voltage dependence of the line broadening due to coupling to the continuum (2) changes in the effective mass parameter with voltage (3) effective $\hbar$ dependence (i.e., B dependence) due to either M_p (e.g., exponential suppression

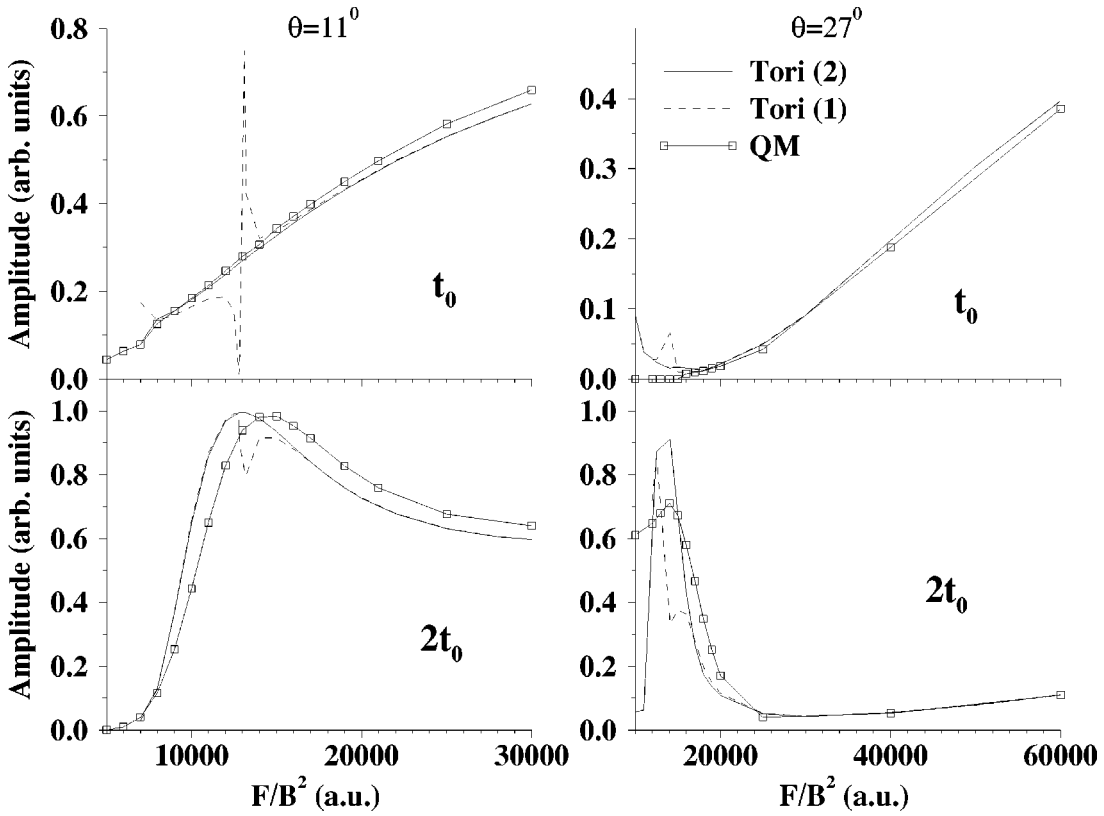

FIG. 9. Quantal (same as in Fig. 7) vs semiclassical comparison in the regular regime. The semiclassical (torus) spectrum is obtained from two models derived from Miller quantization of a large stable island. The solid line represents tori that are just displaced in-plane Landau states with $\beta=\sqrt{B\cos\theta}$. For the broken line, $\beta=\sqrt{\sin 2\pi\nu/m_{12}}$. The torus quantization models agree well except at the bifurcations where $m_{12}=0$. This shows that the whole period-doubling region PD1 at 11° and the 16 000−20 000 range of PD3 are well accounted for by the tori. Hence the S' orbit contribution is not well separated from the t_0 island of stability over part of the PD3 region.

ghosts with $\hbar$) or to the accessibility. The latter suppresses a PO contribution exponentially with $B\cos\theta z_0^2$.

We have analyzed previously unexplained ''jumps'' in the period-one current in stable regions. We have shown these to be due to the dominant current-carrying state stepping up in the $K=0,1,2,\ldots$ torus quantum numbers.

We have introduced a very simple Miller-quantization model that gives excellent agreement with the quantum results. We conclude that any successful theory must as a prerequisite obtain the Miller quantization behavior shown by our torus model in the large ϵ limit.

We conclude that the semiclassical model we tested is not really valid in this experimental regime. It gives poor results, mainly since the condition $|\partial^2\tilde{S}/\partial {z_0}^2|\gg 1$ is not valid over most of our range. Further work indicates that it is possible to relax this condition [21] and hence to derive a more universally valid formula, including the torus limit.

The validity of this semiclassical theory (even in its generalized form) will hinge partly on the validity of the $P_z=0$ selection rule. It is in this aspect, perhaps, that the semiclassical theory of the current differs most from the Gutzwiller trace formula.

To date none of the dozen or so studies of this system has provided convincing evidence of a contribution from an orbit with $P_z\neq 0$. We have not found any in the regimes we considered though in many cases such orbits would not be resolvable from the main POs for which $P_z=0$. This selection rule may explain why so few POs dominate the current, while many orbits are seen in FT's of the density of states (see [6]) even allowing for accessibility constraints. Further experiments may be needed to target the regimes where such orbits are not masked by $P_z=0$ orbits.

This work shows that the current is dominated by ghosts over about half of PD3 as well as the whole of the region between PD1 and PD2. Since the contribution of a ghost should decay extremely rapidly with distance from a bifurcation this is very surprising and is perhaps the most important question to be addressed in future work.

Our calculations show that there are two especially significant bifurcations at 11°: the first period-doubling bifurcation (which produces PD1) and the tangent bifurcation (which leaves a ghost). The second period-doubling bifurcation of t_0 plays a weaker role but interferes slightly with the S_1 contribution at low ϵ. In general, we note that most bifurcations are not detected, neither in the quantum calculation nor in the experiment. Only those bifurcations that produce an enhancement that spans several I-V oscillations (hence have $m_{21}\sim 0$ over a broad region of ϵ), are easily seen experimentally. The ''failed bifurcation'' of S_1 becomes an actual bifurcation for a small increase of injection energy (from $\mathcal{R}=0.15$ to $\mathcal{R}=0.2$). Given uncertainties in experimental parameters one cannot entirely rule out a bifurcation in the experiment. At 27° three bifurcations of S' are present but the current peaks at the synchronous bifurcation at $\epsilon=13\,600$.

ACKNOWLEDGMENTS

We are greatly indebted to Greg Boebinger for providing us with his experimental data. We thank E. Bogomolny, D. Delande, E. Narimanov, and D. Rouben for helpful discussions. We thank E. Narimanov especially for pointing out to us the nature of the cusp bifurcation. T.S.M. acknowledges funding from the EPSRC. D.S.S. acknowledges the financial support from TMR.

APPENDIX A: MONODROMY MATRIX

We consider an orbit $\boldsymbol{\eta}(t)=(z,p_z,x,p_x)(t)$ starting on a surface of section (SOS) $\{x=d,p_x>0\}$ at a point $\boldsymbol{\eta}^0$, and which hits the SOS again at time τ. Writing $\boldsymbol{\mu}=(z,pz)$ the coordinates on the SOS, we define the reduced monodromy matrix $M=(M_{ij}),i,j=1,2$ by

$$M_{ij}=\frac{\partial \mu_i}{\partial \mu_j^0}(\boldsymbol{\mu}^0;\tau)|_{x=d,\ E=\mathrm{cst}} \tag{A1}$$

for a constant energy E. We consider a SOS taken on either the left $(d=0)$ or right $(d=L)$ barrier. As we are interested in periodic orbits, we shall consider Eq. (A1) after a whole period. We divide the trajectory in l continuous partial trajectories between each successive bounce that occur at $d=0$ or $d=L$. For each partial trajectory, we compute a monodromy matrix $M^{(k)},k=1,..,l$ given by relations similar to Eq. (A1). The effect of each bounce is simply to redefine new initial conditions for $M^{(k)}$. Finally,

$$M=\prod_{k=1}^{l} M^{(k)}.$$

Some care has to be taken when evaluating Eq. (A1), as the conditions $x=d,E=\mathrm{const}$ yield some dependence between the arguments $(z^0,p_z^0,d,p_x^0;\tau)$ of M. We have

$$E=\mathrm{const}\Rightarrow p_x^0=p_x^0[z^0,p_z^0,x^0;E]$$

and $x(\boldsymbol{\eta}^0;\tau)=d$ that we solve numerically to get

$$\tau=\tau[\boldsymbol{\eta}^0;d].$$

This means that Eq. (A1) is not evaluated with p_x^0 and τ constant. To see what happens, let us take an example with $j=1$. We have

$$\begin{aligned}M_{i1}&=\left(\frac{\partial \mu_i}{\partial z^0}(z^0,p_z^0,x^0,p_x^0[\ldots;E];\tau[\boldsymbol{\eta}^0;d])\right)_{p_z^0,x^0,d,E}\\&=\left(\frac{\partial \mu_i}{\partial z^0}(\boldsymbol{\eta}^0;\tau)\right)_{p_z^0,x^0,p_x^0,\tau}+\left(\frac{\partial \mu_i}{\partial p_x^0}(\boldsymbol{\eta}^0;\tau)\right)_{z^0,p_z^0,x^0,\tau}\\&\quad\times\left(\frac{\partial p_x^0}{\partial z^0}[z^0,p_z^0,x^0;E]\right)_{p_z^0,x^0,E}\\&\quad+\left(\frac{\partial \mu_i}{\partial \tau}(\boldsymbol{\eta}^0;\tau)\right)_{\boldsymbol{\eta}^0}\left(\frac{\partial \tau}{\partial z^0}[\cdots]\right)_{p_z^0,x^0,E,d}\end{aligned} \tag{A2}$$

and

$$\begin{aligned}\left(\frac{\partial \tau}{\partial z^0}[\cdots]\right)_{p_z^0,x^0,E,d}&=\left(\frac{\partial \tau}{\partial z^0}[\cdots]\right)_{p_z^0,x^0,p_x^0,d}\\&\quad+\left(\frac{\partial \tau}{\partial p_x^0}[\cdots]\right)_{z^0,p_z^0,x^0,d}\\&\quad\times\left(\frac{\partial p_x^0}{\partial z^0}[\cdots]\right)_{p_z^0,x^0,E}.\end{aligned} \tag{A3}$$

From $(dx/dz^0)(\boldsymbol{\eta}^0;\tau)=0$ for $x=d=\mathrm{const}$, we find that

$$\left(\frac{\partial \tau}{\partial z^0}[\cdots]\right)_{p_z^0,x^0,p_x^0,d}=-\frac{[(\partial x/\partial z^0)(\cdots)]_{p_z^0,x^0,p_x^0;\tau}}{[(\partial x/\partial \tau)(\cdots)]_{\boldsymbol{\eta}^0}} \tag{A4}$$

and similarly for $((\partial\tau/\partial p_x^0)[\cdots])_{p_z^0,x^0,p_x^0,d}$. Finally, with $\dot{\boldsymbol{\eta}}(\tau)=[(\partial\boldsymbol{\eta}/\partial\tau)(\boldsymbol{\eta}^0;\tau)]_{\boldsymbol{\eta}^0}$, Eqs. (A2)–(A4) give

$$\begin{aligned}M_{i1}&=\frac{\partial \mu_i}{\partial z^0}(\tau)+\frac{\partial \mu^i}{\partial p_x^0}(\tau)\frac{\partial p_x^0}{\partial z^0}\\&\quad-\frac{\dot{\mu}_i}{\dot{x}}(\tau)\left[\frac{\partial x}{\partial z^0}(\tau)+\frac{\partial x}{\partial p_x^0}(\tau)\frac{\partial p_x^0}{\partial z^0}\right],\end{aligned}$$

where the partial derivatives are now without any ambiguity. M_{i2} is given by the obvious replacement of z^0 by p_z^0.

[1] T. M. Fromhold *et al.*, Phys. Rev. Lett. **72**, 2608 (1994).

[2] G. Muller, G. S. Boebinger, H. Mathur, L. N. Pfeiffer, and K. W. West, Phys. Rev. Lett. **75**, 2875 (1995).

[3] D. L. Shepelyansky and A. D. Stone, Phys. Rev. Lett. **74**, 2098 (1995).

[4] T. S. Monteiro and P. A. Dando, Phys. Rev. E **53**, 3369 (1996).

[5] P. B. Wilkinson, T. M. Fromhold, and L. Eaves, Nature (London) **380**, 608 (1996); T. M. Fromhold *et al.*, Phys. Rev. Lett. **75**, 1142 (1995).

[6] T. S. Monteiro, D. Delande, A. J. Fisher, and G. S. Boebinger, Phys. Rev. B **56**, 3913 (1997).

[7] E. Narimanov and A. D. Stone, e-print cond-mat/9704083.

[8] Fromhold *et al.*, Phys. Rev. Lett. **78**, 2865 (1997).

[9] E. Narimanov, A. D. Stone, and G. S. Boebinger, Phys. Rev. Lett. **78**, 2866 (1997).

[10] T. S. Monteiro, D. Delande, and J. P. Connerade, Nature (London) **387**, 863 (1997).
[11] M. Gutzwiller, *Chaos in Classical and Quantum Mechanics* (Springer-Verlag, New York, 1990).
[12] J. Gao, J. B. Delos, and M. Baruch, Phys. Rev. A **46**, 1449 (1992).
[13] J. Gao and J. B. Delos, Phys. Rev. A **46**, 1455 (1992).
[14] P. A. Dando, T. S. Monteiro, D. Delande, and K. T. Taylor, Phys. Rev. Lett. **74**, 1099 (1995).
[15] E. B. Bogomolny, Zh. Eksp. Teor. Fiz. **96**, 487 (1989) [Sov. Phys. JETP **69**, 275 (1989)].
[16] E. B. Bogomolny and D. C. Rouben (unpublished).
[17] J. Bardeen, Phys. Rev. Lett. **6**, 57 (1961).
[18] M. Kus, F. Haake, and D. Delande, Phys. Rev. Lett. **71**, 2167 (1993).
[19] W. Miller, J. Chem. Phys. **63**, 996 (1975).
[20] T. M. Fromhold *et al.*, Phys. Rev. B **51**, 18 029 (1995).
[21] D. C. Rouben and E. B. Bogomolny (private communication).